Investigating the origin of candidate lava channels on Mercury with MESSENGER data: Theory and observations

Debra M. Hurwitz,[1,2] James W. Head,[1] Paul K. Byrne,[3] Zhiyong Xiao,[4,5] Sean C. Solomon,[3,6] Maria T. Zuber,[7] David E. Smith,[7,8] and Gregory A. Neumann[8]

Received 12 April 2012; revised 31 August 2012; accepted 1 November 2012; published 31 March 2013.

[1] Volcanic plains identified on Mercury are morphologically similar to lunar mare plains but lack constructional and erosional features that are prevalent on other terrestrial planetary bodies. We analyzed images acquired by the MESSENGER spacecraft to identify features on Mercury that may have formed by lava erosion. We used analytical models to estimate eruption flux, erosion rate, and eruption duration to characterize the formation of candidate erosional features, and we compared results with analyses of similar features observed on Earth, the Moon, and Mars. Results suggest that lava erupting at high effusion rates similar to those required to form the Teepee Butte Member of the Columbia River flood basalts ($0.1–1.2 \times 10^6$ m^3 s^{-1}) would have been necessary to form wide valleys (>15 km wide) observed in Mercury's northern hemisphere, first by mechanical erosion to remove an upper regolith layer, then by thermal erosion once a lower rigid layer was encountered. Alternatively, results suggest that lava erupting at lower effusion rates similar to those predicted to have formed Rima Prinz on the Moon (4400 m^3 s^{-1}) would have been required to form, via thermal erosion, narrower channels (<7 km wide) observed on Mercury. Although these results indicate how erosion might have occurred on Mercury, the observed features may have formed by other processes, including lava flooding terrain sculpted during the formation of the Caloris basin in the case of the wide valleys, or impact melt carving channels into impact ejecta in the case of the narrower channels.

Citation: Hurwitz, D. M., J. W. Head, P. K. Byrne, Z. Xiao, S. C. Solomon, M. T. Zuber, D. E. Smith, and G. A. Neumann (2013), Investigating the origin of candidate lava channels on Mercury with MESSENGER data: Theory and observations, *J. Geophys. Res. Planets*, *118*, 471–486, doi:10.1029/2012JE004103.

1. Introduction

[2] The first images of the surface of Mercury by the Mariner 10 spacecraft, with resolutions ranging from ~100 m to tens of kilometers per pixel, revealed the presence of extensive plains of smooth materials within and surrounding the Caloris impact basin as well as on the floors of other smaller basins. These smooth plains were hypothesized to have originated either as basin ejecta materials [*Wilhelms*, 1976] and impact melt and ejecta deposits similar to those found at the Apollo 16 landing site on the Moon [e.g., *Oberbeck et al*., 1977], or as volcanic deposits [*Murray et al*., 1975; *Trask and Guest*, 1975; *Strom et al*., 1975; *Strom*, 1977; *Dzurisin*, 1978; *Kiefer and Murray*, 1987; *Robinson and Lucey*, 1997]. A volcanic origin for these plains was recently supported by analyses of images obtained during the three Mercury flybys by the MErcury Surface, Space ENvironment, GEochemistry, and Ranging (MESSENGER) spacecraft [*Head et al*., 2009]. Since the insertion of MESSENGER into orbit around Mercury in March 2011, analyses of Mercury Dual Imaging System (MDIS) images, obtained at resolutions ranging from ~30 to ~200 m/pixel, as well as Mercury Laser Altimeter (MLA) topography data, have extended the known distribution of smooth volcanic plains on Mercury [*Head et al*., 2011; *Zuber et al*., 2012]. Broad regions of smooth volcanic plains have been observed to preferentially flood low-lying regions such as those near the north pole and inside and outside large impact basins [e.g., *Head et al*., 2011; *Byrne*

[1]Department of Geological Sciences, Brown University, Providence, Rhode Island, USA.
[2]Now at Lunar and Planetary Institute, Universities Space Research Association, Houston, Texas, USA.
[3]Department of Terrestrial Magnetism, Carnegie Institution of Washington, Washington, DC, USA.
[4]Lunar and Planetary Laboratory, University of Arizona, Tucson, Arizona, USA.
[5]Faculty of Earth Sciences, China University of Geosciences (Wuhan), Wuhan, Hubei, P. R. China.
[6]Lamont-Doherty Earth Observatory, Columbia University, Palisades, New York, USA.
[7]Department of Earth, Atmospheric, and Planetary Sciences, Massachusetts Institute of Technology, Cambridge, Massachusetts, USA.
[8]Solar System Exploration Division, NASA Goddard Space Flight Center, Greenbelt, Maryland, USA.

Corresponding author: D. M. Hurwitz, Lunar and Planetary Institute, Universities Space Research Association, Houston, TX 77058, USA. (hurwitz@lpi.usra.edu)

2169-9097/13/2012JE004103

et al., 2011, Byrne et al. (2013), An assemblage of lava flow features on Mercury, *J. Geophys. Res.*, submitted].

[3] The volcanic plains observed on Mercury have morphologies similar to the mare basaltic plains that flood large impact basins and other areas on the Moon [e.g., *Head*, 1976; *Head and Wilson*, 1992; *Whitten et al*., 2011]. Smooth plains include broad expanses of relatively flat terrain on Mercury that show evidence for flow lobes and margins [e.g., *Prockter et al*., 2010; *Head et al*., 2011] as well as faulting that postdates plains emplacement [e.g., *Watters et al*., 2009a, 2009b; *Zuber et al*., 2010]. Smooth plains on both the Moon and Mercury typically lack evidence for specific vents that fed the observed flows [e.g., *Head et al*., 2011]. This lack of resolvable vents is consistent with plains formation by the emplacement of low-viscosity lava that flooded and covered the associated source vents in the interior regions of the flood plains [e.g., *Head et al*., 2011]. However, unlike the Moon, volcanic constructs similar to the Marius Hills [e.g., *Whitford-Stark and Head*, 1977] and eroded features similar to Rima Prinz [*Wilson and Head*, 1980; *Hurwitz et al*., 2012] have not been documented in the flood plains of Mercury [e.g., *Head et al*., 2011; *Byrne et al*., 2011; *Fassett et al*., 2011], perhaps indicative of differences between Mercury and the Moon in mantle dynamics or melt transport [e.g., *Head et al*., 2011; *Wilson and Head*, 2012]. Nonetheless, several features with morphologies similar to those of lunar sinuous rilles and of wider channels like Athabasca Valles on Mars have been observed in high-resolution MDIS images. These features may have formed as the result of erosion of the substrate by fluid impact melt or lava.

[4] Here we present an investigation of the potential for lava to erode the surface of Mercury during the formation of sinuous rille-like features and wider channels. Observations and estimates of channel morphology, specifically channel width and depth, are used as constraints in analytical models for channel formation by mechanical [*Sklar and Dietrich*, 1998] and thermal [*Williams et al*., 1998] erosion. Model results indicate the type of erosion likely to have dominated the evolution of candidate channels and provide estimates of the eruption flux and duration, the lava flow velocity, and the erosion rate that would have been required to form the observed features by lava erosion. This analysis provides insight into how lava erosion, a process that has acted throughout the inner solar system [*Hulme*, 1973; *Wilson and Head*, 1981, 1997; *Head and Wilson*, 1986; *Williams et al*., 1998, 2000, 2001, 2005; *Hurwitz et al*., 2010, 2012], might have operated on the surface of Mercury.

2. Observations

[5] We have identified from MDIS images several candidates for lava erosional features on the surface of Mercury. The candidate features on Mercury vary more widely in morphology than those on the Moon. Some are manifest as narrow and sinuous channels (e.g., Figure 1) that have characteristics similar to those of lunar sinuous rilles, including laterally parallel and continuous walls and meandering traces, and appear to have been incised into the underlying terrain. In contrast, the largest features on Mercury that are candidates for having formed as the result of erosion by lava are four valleys to the south of the southern margin of the northern volcanic plains, near 60°N, 120°E (Figure 2a) [the "broad channels" described by Byrne et al., submitted, 2013]. These valleys range in length from approximately 100 to 250 km, in width from 18 to 25 km, and in depth from 500 m to more than 1 km (Table 1). The valley floors have a much smoother surface than the material outside (e.g., Figure 2b) and contain features such as grooves that curve parallel to valley walls and streamlined mounds oriented parallel to valley walls that appear to have acted as topographic obstructions to flow. These features are consistent with lava flowing approximately from northwest to southeast through the valleys (e.g., Figures 2b and 2c), a flow direction that is inferred from the orientation of the mounds and associated valley distributaries that are likely to have developed downstream in a lava flow that originated at a distinct volcanic source [e.g., *Carr*, 1974]. In the case of the southwestern-most valley (valley 1, located at 59°N, 110°E; Figures 2b, 2c, Table 1), two potential sources are observed northwest of the valley: A pit with a low-relief rim and a depth of 1 km (feature S in Figure 2c, Figure 3), and a smaller pit that is southeast of the first and adjacent to a mountain-like structure, possibly related to the rim of an embayed crater (feature S′ in Figure 2c). The lavas within the other valleys (valley 2, 61.3°N, 115°E; valley 3, 66.3°N, 125°E; valley 4, 63.2°N, 129°E, Figure 2a) are interpreted to have originated in the volcanic plains to the north. Valleys 3 and 4 are characterized by a series of interconnected valleys and craters that exhibit evidence of flooding by lava (Figure 2a).

[6] It should be noted that the floors of these valleys do not decrease monotonically in elevation "downhill" in the direction of original flow [Byrne et al., submitted, 2013]. Some of the variations in topography along the channel may have been constructional in origin as a result of variations in lava fill thickness along the length of the valley. However, the similarity between cross-sections of long-wavelength topography along the valleys and parallel cross-sections of the terrain outside the valleys supports the inference that changes to the long-wavelength topography occurred in this region [*Solomon et al*., 2012]. In our analyses, the lava was assumed to have flowed initially down a nearly level surface having a mean slope that is taken to be a free variable, and processes that occurred after valley formation were assumed to have subsequently modified the slope of the region but to have played no role in valley formation by lava erosion.

[7] Each valley system terminates in an impact basin that is partially filled with lava (Figure 2a). Valley 1 terminates in the partially filled Kofi peak-ring basin that has a diameter of ~135 km (Figure 4a). The volume of fill material can be estimated by comparing the volume of the unfilled portion of Kofi basin with the volume of a fresh basin of a similar diameter (e.g., Eminescu basin, 11°N, 114°E) (Figure 4b) [*Schon et al*., 2011; *Baker et al*., 2011]. The difference between the volume of the fresh Eminescu basin (2.4×10^4 km^3) and the volume of the unfilled portion of Kofi basin (9.3×10^3 km^3) yields an estimated volume of fill material of 1.5×10^4 km^3.

[8] It has been noted previously that these valleys are oriented approximately radial to the Caloris basin, a 1525 km × 1315 km impact basin located ~1000 km to the southeast (centered at 31°N, 160°E) [e.g., *Fassett et al*., 2009, Figure 6]. The radial orientation of the valleys is consistent with their formation as the result of sculpture during

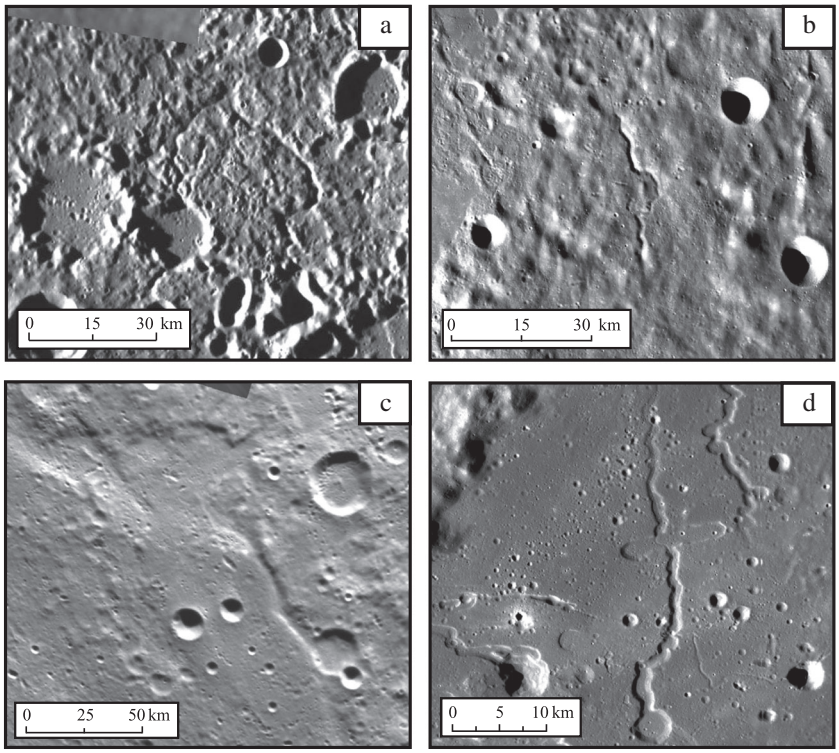

Figure 1. Comparison between candidate lava channels on Mercury and sinuous rilles on the Moon that are interpreted to have formed by lava erosion. (a) Channel at 25°S, 328°E (channel 5 in Table 1), on Mercury; (b) channel located at 53.5°N, 327.5°E, in ejecta materials associated with the northern rim of Imbrium basin on the Moon; (c) channel at 72°S, 167.5°E (channel 8 in Table 1), on Mercury; and (d) Rimae "Handel" and "Telemann," east of Rima Prinz and the Harbinger Mountains on the Moon at 26.7°N, 317.1°E. Features on both bodies have parallel, laterally continuous walls that are consistent with formation by lava erosion in a surface channel [e.g., *Hurwitz et al*., 2012]. Channels in Figures 1a and 1b lack obvious source vents and terminal deposits. Channels in Figures 1c and 1d have nearly circular depressions near their up-slope, southern extents, suggesting that these depressions may have been sources for these channels. North is up in these images and all others in this paper; images are shown in a sinusoidal projection unless otherwise indicated.

Caloris basin formation, followed by lava emplacement that subsequently filled these presculpted valleys. Observations of smoothed and textured islands on the flooded valley floors (e.g., Figure 2) suggest that at least some valley modification occurred as the result of lava flow, and thus erosion by lava is considered as an end-member scenario for the formation of these valleys. The estimated volume of lava in Kofi basin was assumed to represent the volume of lava that flowed through and carved this particular valley. An alternative scenario of a constructional origin for this valley, by which a cooling flood of lava formed levees that bounded the fastest moving part of the flow into a channel, is inconsistent with observations of large valley depths and widths [*Hulme*, 1974; *Hurwitz et al.*, 2013]. The observed valley geomorphology instead indicates that erosion occurred, and thus for this study we investigated the end-member scenario of formation by lava erosion.

[9] Other candidate lava channels on the surface of Mercury are markedly narrower than the northern valley systems, ranging in length from 40 to 80 km and in width from 1 to 6 km (Figures 5–7). Four such channels are located south of 25°S, where there is no topographic information from MLA because of MESSENGER's highly eccentric orbit and northern periapsis. Estimates of channel depth made from shadow measurements suggest that channel depths range from 400 to 800 m. A range of regional slopes on which the channels formed is considered as in the case for the wider channels.

[10] One of the narrow channels (channel 5 in Table 1; 25°S, 328°E, Figure 5) is located in the ejecta of a large, degraded impact, a setting similar to that for many lunar sinuous rilles, e.g., Rima Prinz [*Hurwitz et al*., 2012]. This channel branches into two segments (channels 5W and 5E), and both segments appear to be superposed by impact craters, masking the channel termination. The channel lacks a depression that might be a candidate for an eruptive source, an observation that suggests this channel may have formed from the accumulation and flow of impact melt material rather than from magma. However, as the termini of the channel branches are concealed by ejecta from younger impacts, it is also possible that the source is obscured as well. Therefore, lava erosion was considered to be a possible origin for this feature in the analysis that follows.

[11] Another pair of narrow channels (channels 6 and 7 in Table 1; ~32.6°S, 270.4°E and ~32.9°S, 271.4°E; Figure 6) is similarly located in ejecta material from a large, degraded

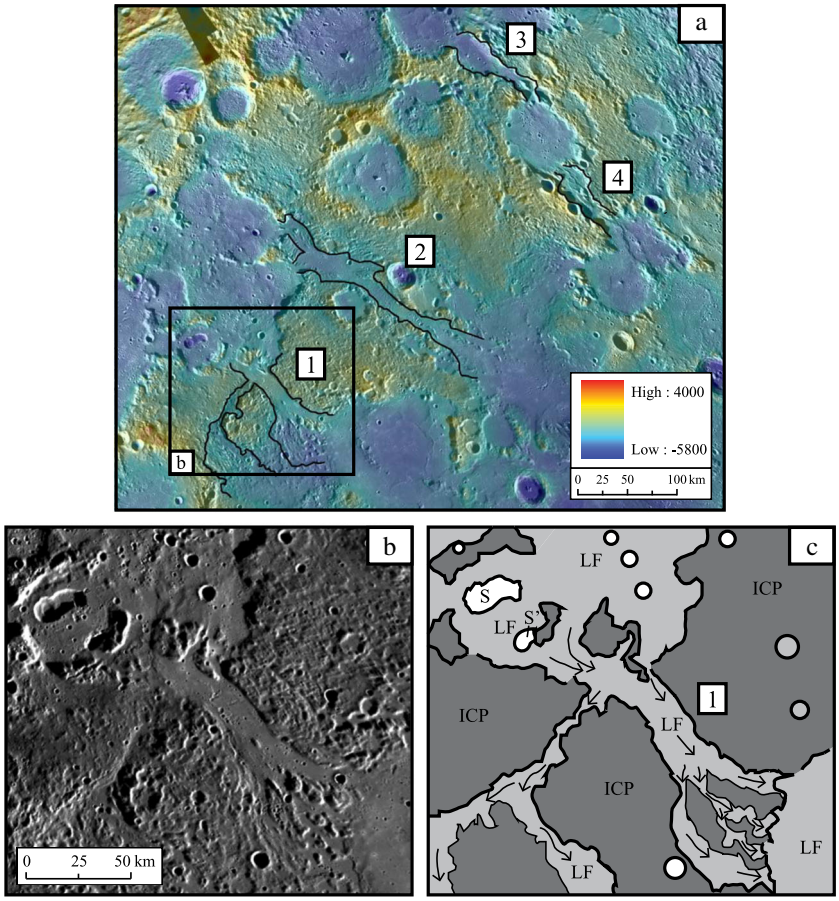

Figure 2. (a) Spatial context for the four wide valleys listed in Table 1, shown with MLA gridded data overlaid on a wide-angle camera (WAC) mosaic centered near 62°N, 120°E. Images are shown in a north polar stereographic projection. Each valley (outlined in black and numbered according to Table 1) typically originates at the rim of a flooded impact basin to the northwest and terminates in another flooded basin to the southeast (valleys 2–4). The boundaries of panels (b) and (c) are shown by a black box. (b) Valley 1 (59°N, 110°E) displays floor material that is smoother than the rougher material outside the valley walls, a characteristic of all four valleys. (c) A geological sketch map of the region surrounding valley 1. Valley 1 may have originated at either of two rimless pits (S, S′), both of which could have fed the volcanic eruption that flooded and potentially carved this valley. Units mapped include intercrater plains (ICP), lava flow (LF), and two candidate source pits (S, S′).

Table 1. Morphometry of Candidate Lava Channels on Mercury

Channel	Channel Segment	Figures	Latitude	Longitude	Channel Length	Channel Width	Channel Depth	Area of Potential Source
			°N	°E	km	km	m	km^2
1	Large valley	2b, 2c	59	110	180	18	500	240
2	Large valley northeast of valley 1	2a	61.3	115	260	18	790	-
3	Large valley north of valley 2; northern segment	2a	66.3	125	120	21	1000	-
4	Large valley southeast of valley 3; southern segment	2a	63.2	129	86	25	1100	-
5W	Western branch of small channel	1a, 5	–25	328	58	2.3	450	20
5E	Eastern branch of small channel	1a, 5	–25	328	60	2.8	420	20
6	Western branch of western small channel	6	–32.6	270.4	84	2.7	860	95
7	Eastern small channel	6	–32.9	271.4	43	1.5	480	44
8	Small channel	1c, 7	–72	167.5	45	6.5	710	290

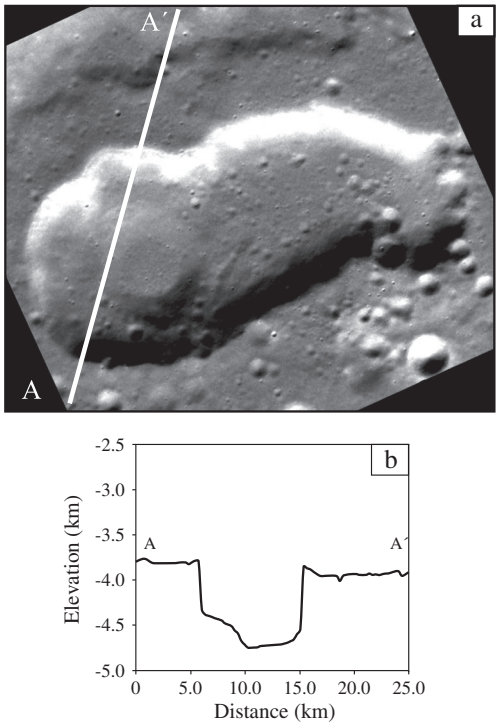

Figure 3. (a) One of two candidate sources for valley 1, shown in narrow -angle camera image EN0218884006M. The line A–A′ denotes the location of the MLA profile in (b), taken from MLA track 1109082009. The candidate source is a pit with steep walls and a multilevel floor. A wide, low-relief rim surrounds the pit; the rim may have been formed by the deposition of particulate material erupted from the vent. (b) The MLA topographic profile (10:1 vertical exaggeration), a segment of MLA track 1109092009, shows the pit's steep walls and relatively flat floors.

impact basin. Elongate depressions at the northwestern ends of these channels may be volcanic sources, though these depressions could also be chains of secondary craters associated with another unrelated impact basin. In a manner similar to the channel shown in Figure 5, the termini of these channels and any associated deposits appear to be concealed by ejecta from younger impact craters.

[12] A fourth candidate for a narrow lava channel (channel 8, Table 1; 72°S, 167.5°E; Figure 7) occurs in smoother intercrater plains materials that differs from materials that host other narrow channels described above. This channel appears to originate in a shallow, flat-floored depression similar to those observed at the heads of some sinuous rilles on the Moon, although this feature on Mercury could be a partially filled impact crater rather than a volcanic source depression. The candidate channel appears to be less degraded by subsequent impact craters than the other narrow channels described above, and it terminates in a topographic low that may contain associated deposits. This candidate lava channel has some characteristics that are similar to those of the surface expression of a thrust fault, e.g., the western wall may coincide with the east-facing leading edge of a small topographic rise that could correspond to a fault-related fold. Nonetheless, the channel shows no evidence of deformation, and the feature was therefore considered as another candidate for formation by lava erosion.

[13] Although some of the features described here may have formed at least in part by impact processes, this study focuses on the end-member case of erosion by lava in order to determine the rate at which lava would have been expected to erode the surface and the duration of the associated eruption that would have been required to form the observed channels. We then compare the results of such analysis for these features on Mercury with analogous features on other planetary bodies.

3. Modeling Lava Erosion on Mercury

3.1. Introduction to Models of Mechanical and Thermal Erosion

[14] Measurements and estimates of channel width, depth, and regional slope, as well as estimates of deposit volumes where available, were used as inputs in analytical models to estimate eruption fluxes and durations, flow velocity, and erosion rates. These models were applied to investigate the possible origin of one representative wide valley (channel 1 in Table 1 and Figure 2b) and one representative narrow channel (channel 5E in Table 1 and Figure 5b) to compare how formational processes might have differed between the two types of features. Two mechanisms of erosion were considered in the formation of these features: Mechanical erosion, which occurs as the result of collisions between particles in the flowing lava and the substrate, and thermal erosion, which occurs when the flowing lava is sufficiently hot to melt and entrain the substrate. These two erosional regimes are likely to occur simultaneously as the hot lava erodes partially melted material via thermo-mechanical erosion [e.g., *Fagents and Greeley*, 2001]; however, these processes are investigated independently here to determine their relative efficiencies during the formation of candidate lava channels on Mercury.

[15] To solve for erosion rate, lava flow velocity must first be determined. Velocity was calculated using a model defined by *Williams et al*. [1998], given by

$$(v_{\mathrm{lava}})^2 = \frac{4\, g\, d_{\mathrm{lava}} \sin \alpha}{C_{\mathrm{f}}}, \tag{1}$$

where C_{f} is a friction factor defined [*Williams et al*., 2001] by

$$C_{\mathrm{f}} = [0.79 \ln(2\, Re) - 1.64]^{-2}. \tag{2}$$

[16] In these equations, g is the surface gravitational acceleration of Mercury (3.7 m s^{-2}), d_{lava} is the depth of the lava within the channel, α is the regional slope, Re is the Reynolds number ($Re = (\rho\, v_{\mathrm{lava}}\, d_{\mathrm{lava}})/\mu_{\mathrm{lava}}$; turbulent flow that promotes erosion occurs when $Re > 2000$), ρ is the density of the lava, and μ_{lava} is the dynamic viscosity of the lava (see Table 2 for lava parameters). Velocity was found by iteratively solving these equations and adjusting d_{lava} in small increments until a solution was reached for a given regional slope. This model for estimating lava velocity within the channel is specifically applicable to turbulent flow within a wide, noncircular lava tube. An alternative model for determining the lava velocity of a turbulent sheet flow, given by *Keszthelyi and Self* [1998], employs the Chezy formula for lava velocity and a friction

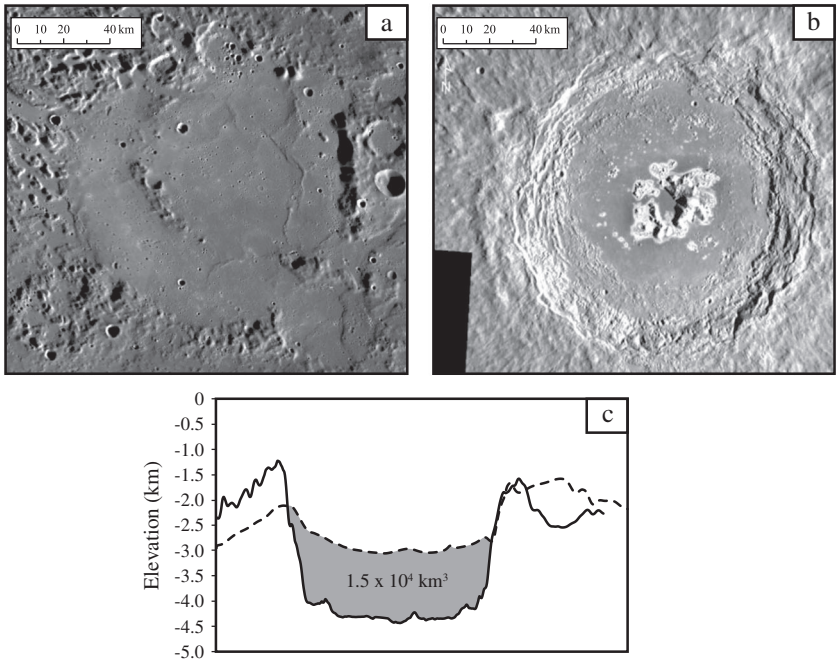

Figure 4. (a) The nearly fully flooded Kofi basin is ~135 km in diameter and is located at the terminus of valley 1 (left side of image). (b) A relatively fresh basin, Eminescu, is similar in diameter to the filled basin in Figure 4a. (c) Topographic profiles across the basins in Figures 4a and 4b. The profile for Kofi basin (dashed line) is from MLA track 1108050842; the profile for Eminescu (solid line) is from the gridded MLA topography [*Zuber et al*., 2012]. The shaded region is a cross-section through the estimated volume of fill material.

coefficient defined by *Goncharov* [1964]. This alternative formulation typically results in a thinner and faster lava flow than the *Williams et al*. [2001] model.

[17] The calculated velocity was then used in models for both mechanical and thermal erosion. The change in channel depth as a result of mechanical erosion is given by

$$\left[\frac{\mathrm{d}(d_{\mathrm{chan}})}{\mathrm{d}t}\right]_{\mathrm{mech}} = K_{\mathrm{g}}\,\rho\,g\,Q_{\mathrm{w}}\sin\alpha, \tag{3}$$

where Q_{w} is the average lava volume flux per unit width through the channel in $\mathrm{m^2\,s^{-1}}$ [given by $Q_{\mathrm{w}} = v_{\mathrm{lava}}\,d_{\mathrm{lava}}$, factors calculated with equations (1) and (2)], and K_{g} is a dimensional ratio (in units of $\mathrm{Pa^{-1}}$) that represents the erodibility of the substrate [*Sklar and Dietrich*, 1998; *Hurwitz et al*., 2010]. The erodibility factor was assumed to be relatively large (i.e., $2.5 \times 10^{-8}\,\mathrm{Pa^{-1}}$) for an unconsolidated substrate such as regolith or loose soil, resulting in a higher rate of erosion; this factor was assumed to be relatively small (i.e., $5 \times 10^{-9}\,\mathrm{Pa^{-1}}$) for a more competent substrate such as dry impact ejecta or basaltic basement, resulting in a lower rate of erosion [e.g., *Hurwitz et al*., 2010]. The model in equation (3) takes into account the potential energy (i.e., $\rho\,g\sin\alpha$) and kinetic energy (i.e., $Q_{\mathrm{w}} = v_{\mathrm{lava}}\,d_{\mathrm{lava}}$) contributed by the flowing lava.

[18] In contrast, thermal erosion is dominated by the thermal energy component contributed by the flowing lava, and the change in channel depth that occurs as the result of thermal erosion has been defined by *Hulme* [1973] and is given by

$$\left[\frac{\mathrm{d}(d_{\mathrm{chan}})}{\mathrm{d}t}\right]_{\mathrm{therm}} = \frac{h_{\mathrm{T}}\left(T - T_{\mathrm{mg}}\right)}{E_{\mathrm{mg}}}, \tag{4}$$

where T and T_{mg} are the initial erupted temperature of the lava (i.e., the liquidus temperature of the lava considered) and the melting temperature of the substrate (i.e., the solidus temperature of the lava considered), respectively, and h_{T} is a heat transfer coefficient. The liquidus temperature is consistently used [e.g., *Williams et al*., 1998, 2001] to estimate the temperature at which lava erupts rapidly from a source located deep in the crust or in the upper mantle before substantial cooling can occur within the lithosphere, as is expected to be the case on the Moon [e.g., *Wilson and Head*, 1981] and, similarly, on Mercury. The term E_{mg} in the denominator of equation (4) is the energy required to melt the substrate and is given by

$$E_{\mathrm{mg}} = \rho_{\mathrm{g}}\left[c_{\mathrm{g}}\left(T_{\mathrm{mg}} - T_{\mathrm{g}}\right) + f_{\mathrm{mg}}L_{\mathrm{g}}\right], \tag{5}$$

where T_{g} is the initial temperature of the ground or substrate, c_{g} is the specific heat of the substrate, and L_{g} is the latent heat of fusion of the substrate. The factor f_{mg} is the fraction that the substrate must be melted before being carried away by the flowing fluid [*Hulme*, 1973; *Williams et al*., 1998], assumed here to be 1. This factor can be varied to account for scenarios in which both mechanical and thermal erosion occur during a flow and erosion event, but here we investigated the end-member case in which thermal erosion occurs independently of mechanical erosion (i.e., $f_{\mathrm{mg}} = 1$) in order to determine the relative efficiency of each mechanism during the lava erosion process on Mercury.

[19] The surface temperature on Mercury encountered by a lava flow can vary by as much as 600 K from day to night because of Mercury's slow rotation (one Mercury day equals ~176 Earth days) and eccentric orbit, but because the channels are likely to take longer than one Mercury day to form, an average temperature of 350 K was assumed

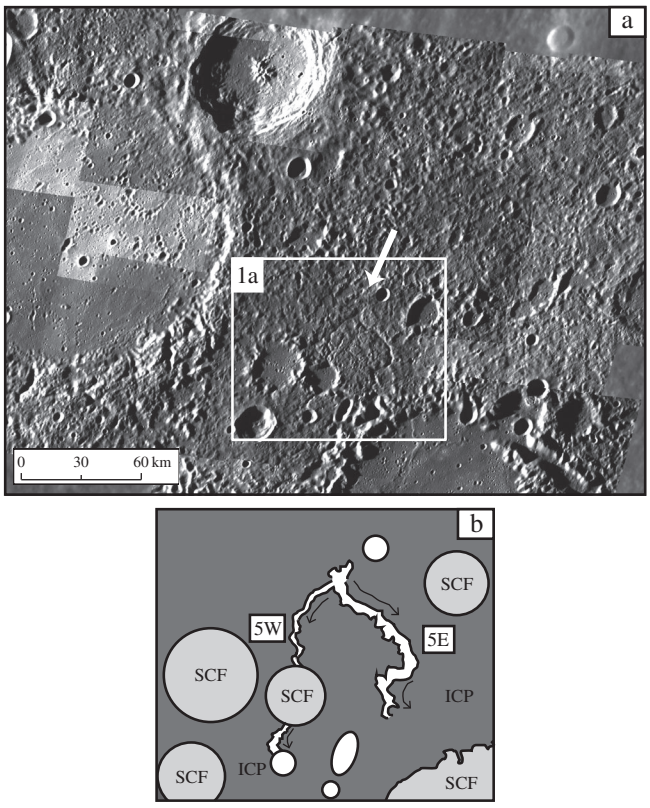

Figure 5. (a) Spatial context for the channel (white arrow, channel 5 in Table 1) shown in Figure 1a in an MDIS WAC mosaic (centered at 25°S, 328°E). The branching channel formed in the ejecta from a large, degraded impact basin. (b) A sketch of the region in the white box in Figure 5a displaying the location and the possible flow direction of the channels in Figure 1a. Associated source vents and terminus deposits are not observed, possibly due to degradation by younger impacts. Units mapped in this study include intercrater plains (ICP) and smooth crater fill (SCF).

[e.g., *Morrison*, 1970; *Paige et al*., 2012]. Analyses with this average surface temperature will yield an average predicted rate of erosion, but a surface with a higher temperature will require less thermal energy to heat the surface to its melting temperature [the first term in equation (5)], and therefore erosion will occur at a higher rate in the presence of such hotter substrate, and vice versa. Initial analyses suggested that an increase in surface temperature by 600 K results in an increase in the modeled thermal erosion rate by ~40% (i.e., a thermal erosion rate of 3.3 m per Earth day, $m\,d^{-1}$, for a komatiite erupting on a surface with a night-time surface temperature of 80 K versus a thermal erosion rate of 5.5 $m\,d^{-1}$ for a komatiite erupting on a surface with a day-time surface temperature of 700 K).

[20] The rate of thermal erosion is governed by the ratio between the thermal energy in the flowing lava and the energy required to melt the substrate [equation (4)]. The heat transfer coefficient in equation (4) represents how efficiently thermal energy can be transferred from the hot flowing lava to the substrate [*Kakaç et al*., 1987; *Williams et al*., 1998] and is given by

$$h_T = \frac{0.027\,k\,Re^{4/5}\,Pr^{1/3}}{d_{lava}}\left(\frac{\mu_b}{\mu_g}\right)^{0.14}, \qquad (6)$$

where k is the thermal conductivity of the lava, μ_b and μ_g are the bulk viscosity of the lava and the viscosity of the melted substrate, respectively, and Pr is the Prandtl number ($Pr = c_g\,\mu_{lava}/k$). Although contributions of thermal energy dominate the thermal erosion process, potential energy and kinetic energy are also incorporated into the model through the Reynolds number in equation (6).

[21] These models were used to investigate the origin of two classes of features, wide valleys and narrow channels, to determine whether mechanical or thermal erosion can be expected to dominate during the formation of eroded lava channels on Mercury, and to determine the effusion rate, the volume of lava, and the time required to form the observed features.

3.2. Modeling the Formation of a Wide Valley

[22] For the wide valley on Mercury labeled as valley 1 in Figure 2 and Table 1, the volume of material that flowed through the channel before being deposited in a partially filled impact basin was estimated to be ~1.5×10^4 km^3 (as explained in section 2). Given this quantity, the velocity was calculated as a function of regional slope for an assumed initial depth of lava within the channel. The erosion rates were then calculated from equations (3)–(6). The duration of the eruption was calculated from the modeled volume flux ($Q = Q_w\,w_{valley}$) and the estimated lava volume, and the modeled depth of erosion was calculated with this duration and the modeled erosion rate. The initial depth of lava within the flowing channel was then adjusted and the

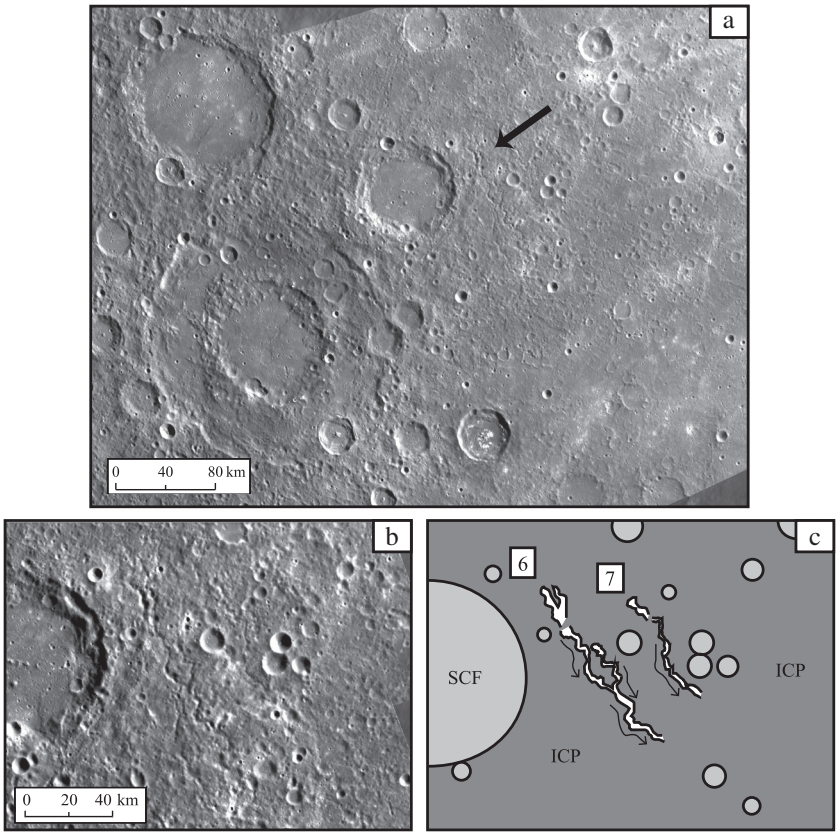

Figure 6. (a) Spatial context for the pair of channels (black arrow, channels 6 and 7 in Table 1) shown in an MDIS WAC mosaic (centered at 32.6°S, 270°E). (b) These two narrow, sinuous channels formed in the ejecta from a large, degraded impact basin. The channels may originate in elongate, partially filled depressions that may be source vents or, alternatively, they may be secondary craters associated with the emplacement of another impact crater. (c) A sketch displaying the locations and possible flow directions of the channels shown in Figure 6b. Units mapped in this study include intercrater plains (ICP) and smooth crater fill (SCF).

models iterated until the modeled depth of erosion matched the observed depth of the valley.

3.3. Modeling the Formation of a Narrow Channel

[23] For the narrow channel considered here (channel 5E in Table 1 and Figures 1a and 5), the volume of material involved is not known, and thus an alternative model was used to estimate the eruption volume flux Q [e.g., *Wilson and Head*, 1980, 1981]. In that model,

$$Q = \frac{5000\, w_{\mathrm{chan}}}{\rho_{\mathrm{lava}}}. \tag{7}$$

[24] Velocity was again calculated as before [equation (1)], but once a depth of lava within the channel and associated velocity were constrained, the modeled volume flux Q was calculated ($Q = Q_{\mathrm{w}}\, w_{\mathrm{valley}}$) and compared with the eruption volume flux [equation (7)]. The depth of lava within the channel was then adjusted and equations (1) and (2) iterated until the modeled volume flux matched the estimated eruption volume flux [equation (7)]. The resulting velocity and lava depth were then used as inputs into the models for mechanical and thermal erosion [equations (3)–(6)] to determine the erosion rates, eruption duration, and lava volume expected for the formation of the channel considered.

3.4. General Assumptions

[25] For both types of channel considered, both the substrate (assumed to be a rigid material) and the flowing lava were assumed to have the same composition, similar to either a terrestrial high-Mg komatiite (i.e., Kambalda, Western Australia, adapted from *Lesher and Arndt* [1995] and *Williams et al.* [1998]) or a terrestrial ocean island basalt (i.e., Kilauea, Hawaii [*Clague et al.*, 1991]). A composition similar to that of a komatiite is considered because this composition has been identified to have a high eruption temperature (<1700 K) and a low viscosity (<1 Pa s) because of its high Mg and low Si contents; lavas with a low viscosity are more likely to flow in a turbulent flow regime and thus are expected to be more efficient erosion agents [e.g., *Hulme*, 1973; *Wilson and Head*, 1981; *Huppert and Sparks*, 1985; *Williams et al.*, 1998, 2001]. A composition similar to that of a terrestrial ocean island basalt was considered because data collected by the X-Ray Spectrometer on MESSENGER suggest that surface materials on Mercury have compositions that are intermediate between those typical of basalts and those typical of more ultramafic materials, and that the northern volcanic

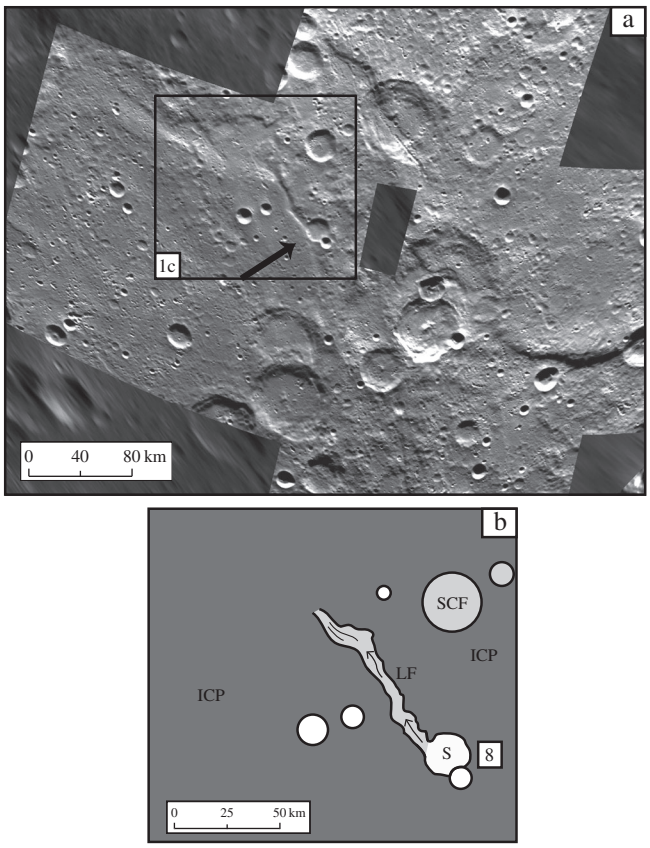

Figure 7. (a) Spatial context for the channel (black arrow, channel 8 in Table 1) shown in an MDIS WAC mosaic (centered at 72°S, 167.5°E) and in Figure 1c. The channel may have originated at a circular, partially filled source depression similar to those observed in association with some sinuous rilles on the Moon (e.g., Figure 1d), but this depression on Mercury may alternatively represent a partially filled impact crater. (b) A sketch of the region in the black box in Figure 7a displaying the location and the possible flow direction of channel 8 in Figure 1c. Units mapped in this study include intercrater plains (ICP), smooth crater fill (SCF), lava flow (LF), and a possible volcanic source (S).

plains are closer to abasaltic composition than the older areas that surround them [*Nittler et al*., 2011; *Weider et al*., 2012]. A composition similar to that of a terrestrial ocean island basalt corresponds to a slightly more viscous lava than a komatiite (see Table 2), and it is illustrative to consider how such a lava behaves differently from one of lower viscosity in the formation of an eroded lava channel on Mercury.

4. Results

[26] The models described in section 3 have been used to simulate the formation of a representative wide valley (valley 1, Table 1) and a representative narrow channel (channel 5E, Table 1). Lava flow velocity and volume flux were calculated, mechanical and thermal erosion rates were modeled, and eruption durations and erupted volumes were determined for each case. For all models involving flow over a compotent substrate, results indicate that thermal erosion for the employed regional slopes would occur at a higher rate than mechanical erosion, suggesting that thermal erosion would have dominated the formation of the features observed on Mercury. If the lava instead flowed over an unconsolidated surface (such as impact ejecta or regolith), the mechanical erosion rate would increase substantially, possibly resulting in an initial stage of incision that would have been dominated by mechanical erosion, reducing the total time expected to form the observed feature. Previous investigations of the origin of lunar sinuous rilles suggested that flow over an unconsolidated substrate would decrease the duration of channel formation by ~10 days, compared with flow over a compotent substrate, if the unconsolidated materials were ~10 m thick [e.g., *Hurwitz et al*., 2010, 2012], such as is thought to be the case for lunar maria [e.g., *Fa and Jin*, 2010; *Kobayashi et al*., 2010]. The thickness of unconsolidated material in the lunar highlands, however, is likely to be much greater than in the lunar maria [e.g., *Hartmann*, 1973]. Model results for each considered scenario are discussed below and are summarized in Figure 9 and Table 3. In the results presented below, duration of formation is given in Earth days (day), where one Earth day is 86,400 s, and the erosion rate (as in the discussion above) is listed in units of meters per Earth day ($m\,d^{-1}$). Formation duration is also given in seconds (s), and erosion rate in units of meters per second ($m\,s^{-1}$), in Table 3.

4.1. Origin of Wide Valleys

[27] Model results for the wide valley (Figure 2) indicate that lava with a composition similar to that of a terrestrial

Table 2. Adopted Model Parameters for Lava and Substrate

Lava Type	Parameter	Unit	Value
Komatiite[a]	Viscosity of lava	Pa s	0.1
	Density of lava	$kg\,m^{-3}$	2770
	Liquidus (initial) temperature of lava	°C	1580
	Solidus (melting) temperature of lava	°C	1170
	Initial temperature of substrate	°C	77
	Specific heat of lava	$J\,kg^{-1}\,K^{-1}$	1790
	Conductivity of lava	$J\,m^{-1}\,s^{-1}\,K^{-1}$	0.4
	Latent heat of lava	$J\,kg^{-1}$	7.0×10^5
	Erodibility of a rigid substrate	Pa^{-1}	5.0×10^{-9}
	Erodibility of an unconsolidated substrate	Pa^{-1}	2.5×10^{-8}
Ocean Island Basalt[b]	Viscosity of lava	Pa s	1.4
	Density of lava	$kg\,m^{-3}$	2760
	Liquidus (initial) temperature of lava	°C	1410
	Solidus (melting) temperature of lava	°C	1050
	Initial temperature of substrate	°C	77
	Specific heat of lava	$J\,kg^{-1}\,K^{-1}$	1630
	Conductivity of lava	$J\,m^{-1}\,s^{-1}\,K^{-1}$	0.5
	Latent heat of lava	$J\,kg^{-1}$	4.2×10^5
	Erodibility of a rigid substrate	Pa^{-1}	5.0×10^{-9}
	Erodibility of an unconsolidated substrate	Pa^{-1}	2.5×10^{-8}

[a]Komatiite parameters were taken from *Hurwitz et al*. [2012], for a simulation using the model developed by *Williams et al*. [1998] with an initial lava composition matching that of komatiitic basalt from Kambalda, W. Australia [*Lesher and Arndt*, 1995].
[b]Ocean Island Basalt parameters were taken from *Hurwitz et al*. [2012], for a simulation using the model developed by *Williams et al*. [1998] with an initial lava composition matching that of a volcanic glass from Kilauea, Hawaii [*Clague et al*., 1991].

komatiite would have been expected to flow down a regional slope of 0.1° at a velocity of $7\,m\,s^{-1}$ and down a slope of 1.0° at a velocity of $23\,m\,s^{-1}$, incising a valley into a solidified substrate by thermal erosion at a rate that ranges from $6.9\,m\,d^{-1}$ to $\sim 17\,m\,d^{-1}$, respectively (Figure 8a and Table 3). A lava flow that eroded at these rates would require a duration of ~30 to ~70 Earth days for 1.0° and 0.1° slopes, respectively, to form a valley of depth 500 m, as observed. An erupted volume of $1.5 \times 10^4\,km^3$ emplaced in ~30 Earth days (i.e., down a 1.0° slope) would need to be supplied at an eruption rate of $6.1 \times 10^6\,m^3\,s^{-1}$, whereas an eruption of a similar lava volume over ~70 Earth days (i.e., down a 0.1° slope) would require an eruption rate of $2.4 \times 10^6\,m^3\,s^{-1}$. In contrast, lava with a composition similar to a terrestrial ocean island basalt would have been expected to flow at a lower velocity that ranged from $4\,m\,s^{-1}$ (on a 0.1° slope) to $12\,m\,s^{-1}$ (1.0° slope), incising a valley by thermal erosion at rates of $1.8\,m\,d^{-1}$ and $4.5\,m\,d^{-1}$, respectively. The slightly lower erosion rate would require more time (~300 Earth days or <1 Earth year where the slope was 0.1° and ~100 Earth days where the slope was 1.0°) to form the observed valley, and a slightly lower eruption flux ($0.6 \times 10^6\,m^3\,s^{-1}$ for a 0.1° slope, $1.6 \times 10^6\,m^3\,s^{-1}$ for a 1.0° slope) to release the observed lava volume of $1.5 \times 10^4\,km^3$. The eruption flux predicted under each of these scenarios is similar to the fluxes estimated for the terrestrial fissure eruption thought to have formed the Teepee Butte Member of the Columbia River Basalt, $(0.1–1.2) \times 10^6\,m^3\,s^{-1}$ [*Reidel and Tolan*, 1992]. These results were calculated using the *Williams et al*. [2001] formulation for lava velocity. Thermal erosion rates tend to be lower, and thus the duration of channel formation is longer, if the lava velocity model defined by *Keszthelyi and Self* [1998] is employed (Figure 8a).

[28] The scenario of lava flowing down a gradient was also considered for an unconsolidated substrate such as a layer of unconsolidated regolith material, similar to the regolith on lunar mare surfaces [e.g., *Fa and Jin*, 2010; *Kobayashi et al*., 2010] and the megaregolith in the lunar highlands [*Hörz et al*., 1991; *Hiesinger and Head*, 2006]. For an unconsolidated regolith substrate, the lava erosion rate by mechanical erosion is substantially greater than for a solidified substrate, ranging from 5.1 to $\sim 130\,m\,d^{-1}$ (for 0.1° and 1.0° slopes, respectively) for a lava similar in composition to a komatiite and ranging from 1.3 to $\sim 30\,m\,d^{-1}$ (for 0.1° and 1.0° slopes, respectively) for a lava similar in composition to an ocean island basalt (Figure 8a and Table 3). If the regolith on the surface of Mercury has an average thickness similar to that on lunar maria, e.g., ~10 m [*Fa and Jin*, 2010; *Kobayashi et al*., 2010], then mechanical erosion would be expected to erode 10 m of regolith in 0.1–2 Earth days due to erosion by a komatiite-like lava and in 0.3–8 Earth days due to erosion by a lava similar in composition to ocean island basalt, decreasing the total time required to form the observed valley from the corresponding solid-substrate cases.

4.2. Origin of Narrow Channels

[29] Model results for the narrow channel (channel 5E in Table 1 and Figures 1a and 5) indicate that lava with a composition similar to a terrestrial komatiite could have flowed along a slope of 0.1° at a velocity of $1.3\,m\,s^{-1}$, thermally eroding a channel into a solid substrate at a rate of $3.0\,m\,d^{-1}$ (Figure 8b). In contrast, lava similar to a terrestrial ocean island basalt would have flowed down the same slope at a slightly lower velocity of $1.6\,m\,s^{-1}$, incising a channel into a solid substrate by thermal erosion at a slightly slower rate of $\sim 0.9\,m\,d^{-1}$. If the regional slope were similar for all the narrow channels, these modeled flow velocities and erosion rates would be the same for all channels, but the time required to form each channel would depend on the channel depth. Results shown in Figure 8b indicate that if the actual slope at the time of channel formation had been steeper than 0.1°, then the flow velocity (Table 3) and thus the modeled erosion rate would be higher, decreasing the

Table 3. Model Results for a Representative Wide Valley and Narrow Channel

Feature	Lava Type	Latitude, Longitude	Slope	Lava Depth	Lava Velocity	Volume Flux[a]	Volume Erupted[a]	Mechanical Erosion Rate	Time for Mechanical Erosion	Mechanical Erosion Rate	Time for Mechanical Erosion	Thermal Erosion Rate	Time for Thermal Erosion
								Competent $K = 5 \times 10^{-9}$		Unconsolidated $K = 2.5 \times 10^{-8}$			
				m	$m\,s^{-1}$	$m^3\,s^{-1}$	km^3	$m\,d^{-1}$ ($m\,s^{-1}$)	Earth days (s)	$m\,d^{-1}$ ($m\,s^{-1}$)	Earth days (s)	$m\,d^{-1}$ ($m\,s^{-1}$)	Earth days (s)
Wide valley (1)	Komatiitic lava	59, 110	0.1	18.0	7.4	2.4×10^6	*15000*	1.0 (1.2×10^{-5})	500 (5.2×10^7)	5.1 (5.9×10^{-5})	100 (8.4×10^6)	6.9 (8.0×10^{-5})	70 (6.3×10^6)
	Basaltic lava	59, 110	0.1	9.0	3.7	0.6×10^6	*15000*	0.3 (3.0×10^{-6})	1900 (1.6×10^8)	1.3 (1.5×10^{-5})	400 (3.3×10^7)	1.8 (2.0×10^{-5})	300 (2.4×10^7)
Narrow channel (5E)	Komatiitic lava	–32, 334.8	0.1	1.3	1.4	*5100*	60	0.01 (1.6×10^{-7})	30,000 (2.6×10^9)	0.07 (8.1×10^{-7})	6000 (5.1×10^8)	3.0 (3.5×10^{-5})	140 (1.2×10^7)
	Basaltic lava	–32, 334.8	0.1	1.6	1.1	*5100*	240	0.01 (1.2×10^{-7})	30,000 (2.6×10^9)	0.07 (8.1×10^{-7})	6000 (5.1×10^8)	0.9 (1.1×10^{-5})	440 (4.8×10^7)
Wide valley (1)	Komatiitic lava	59, 110	1.0	14.9	22.7	6.1×10^6	*15000*	26 (8.3×10^{-5})	20 (1.7×10^6)	130 (1.5×10^{-3})	5 (3.3×10^5)	17 (2.0×10^{-4})	30 (2.5×10^6)
	Basaltic lava	59, 110	1.0	7.6	11.8	1.6×10^6	*15000*	7.0 (8.0×10^{-5})	70 (6.3×10^6)	30 (4.0×10^{-4})	15 (1.2×10^6)	4.5 (5.2×10^{-5})	100 (9.5×10^6)
Narrow channel (5E)	Komatiitic lava	–32, 334.8	1.0	0.6	3.0	*5100*	30	0.1 (1.6×10^{-6})	3000 (2.6×10^8)	0.7 (8.1×10^{-6})	600 (5.1×10^7)	6.5 (7.5×10^{-5})	60 (5.5×10^6)
	Basaltic lava	–32, 334.8	1.0	0.8	2.4	*5100*	90	0.1 (1.6×10^{-6})	3000 (2.6×10^8)	0.7 (8.1×10^{-6})	600 (5.1×10^7)	2.0 (2.3×10^{-5})	200 (1.8×10^7)

[a]Italicized entries indicate parameters that were adopted for the respective model. Volume Flux for the narrow channel was estimated from the expression given by *Wilson and Head* [1981]. Volume Erupted for the wide valley was equated to the volume of lava estimated to have filled Kofi basin.

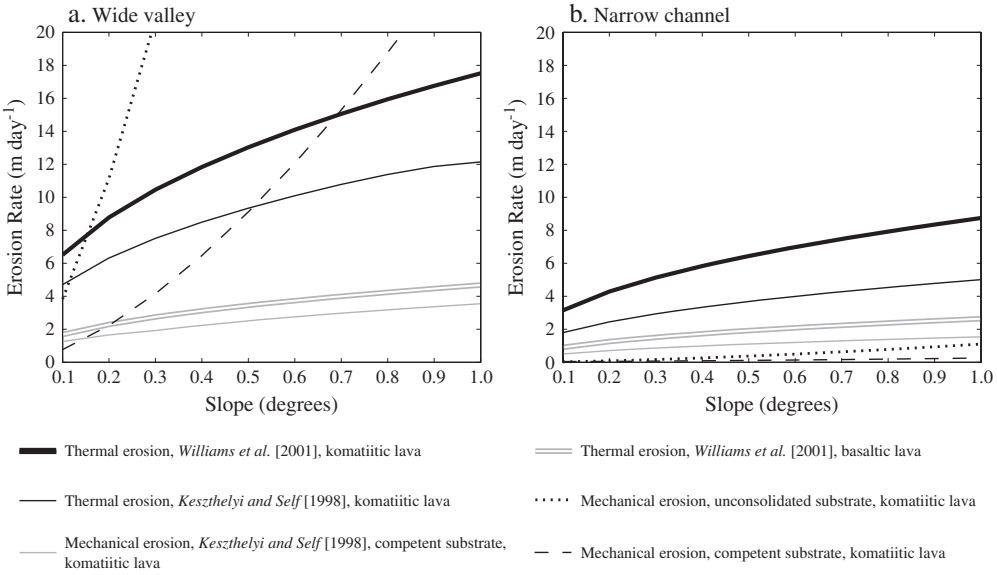

Figure 8. Results of erosion rate in meters per Earth day (m d^{-1}) as a function of slope for a komatiitic or basaltic lava on Mercury eroding by thermal erosion or mechanical erosion into a competent substrate or unconsolidated regolith. The thin solid lines denote results with the velocity model for turbulent sheet lava flows [*Keszthelyi and Self*, 1998]; all other lines show results with the velocity model for turbulent tube lava flows [*Williams et al.*, 2001]. (a) Model results for the formation of a wide valley indicate that the komatiitic lava would have eroded more efficiently than the basaltic lava in all cases. Thermal erosion would have dominated during the formation of the valley at slopes $< 0.7°$ if the substrate had been competent, but mechanical erosion would have dominated during valley formation at slopes $> 0.2°$ if the substrate had been unconsolidated. (b) Model results for the formation of a narrow channel indicate that the komatiitic lava would have eroded more efficiently than the basaltic lava and that thermal erosion would have dominated during the formation of the channel regardless of the competency of the substrate.

amount of time required to form the observed channels, and vice versa. As in the case with the wide valleys, thermal erosion rates tend to be lower if the alternative model for calculating lava velocity [*Keszthelyi and Self*, 1998] is assumed (Figure 8b).

[30] The time required to form these channels depends not only on the regional slope but also on the channel depth. The shallowest channel, according to shadow measurements (channel 5E, 420 m, Table 1), would require ~140 Earth days to form from thermal erosion by a komatiitic lava and ~1.2 Earth years (~440 Earth days) to form from erosion by a basaltic lava, for a 0.1° slope; the deepest channel according to shadow measurements (channel 6, 860 m, Table 1) would have required ~300 Earth days to form by flow of a komatiitic lava and ~2.6 Earth years (~950 Earth days) to form by flow of oceanic island basaltic lava, for a 0.1° slope.

[31] Additional modeling of channel formation by mechanical erosion predicts that mechanical erosion rates would be lower than thermal erosion rates for narrow channels (Figure 8b and Table 3). Therefore, mechanical erosion is not expected to dominate the erosion process during the formation of the narrow channels on shallow regional slopes on Mercury. The efficiency of lava to mechanically erode into an unconsolidated substrate is predicted to have been much lower during the formation of a narrow channel than in the formation of a wide valley (Figure 8). This difference in mechanical erosion efficiency is because of the difference in widths of the observed features: the narrower channel results in a lower calculated lava flow velocity [i.e., equation (1)] and thus a lower rate of erosion than that predicted for the wide valley. The magnitude of lava flow velocity affects mechanical erosion rates [equation (3)] more markedly than it does the thermal erosion rates [equation (4)], and so thermal erosion is expected to have dominated the formation of the narrow channels regardless of substrate consolidation. In contrast, mechanical erosion is expected to have dominated the formation of the wide valleys on Mercury until the upper unconsolidated regolith material was removed, after which thermal erosion is expected to have been the primary incising process.

5. Discussion

[32] Observations of orbital images collected by the MESSENGER spacecraft indicate that volcanic morphologies on the surface of Mercury are commonly manifest as extensive deposits of smooth plains that contain a scarcity of readily identifiable volcanic features [e.g., *Head et al.*, 2011]. This paucity of observed features is consistent with the emplacement of flood lavas that covered eruption sites, effectively burying evidence for most source vents and associated erosional features. The identification of possible source vents associated with several of the features investigated in this study (e.g., valley 1, Table 1 and Figure 2) may indicate that the eruptions in these locations emplaced lava on terrain with a sufficient and regionally consistent slope that lava was able

to incise. In contrast, the density of impact craters in other locations has inhibited this lava emplacement process, instead providing potential locations for lava to pool rather than erode. This outcome would be consistent with the high frequency of impact craters observed to be flooded with lava and the comparative rarity of channelized lava flows observed on the surface of Mercury.

[33] In contrast, features interpreted to have formed by channelized lava flows have been commonly observed on other terrestrial planetary bodies [e.g., *Greeley*, 1971a, 1971b; *Sharp and Malin*, 1975; *Masursky et al*., 1977; *Strain and El-Baz*, 1977; *Carr and Clow*, 1981; *Head et al*., 1992; *Komatsu et al*., 1992, 1993; *Komatsu and Baker*, 1992], and many of these features are generally thought to have formed as the result of high-flux, point-source eruptions of lava that may have been characterized by high temperatures and low viscosities [e.g., *Hulme*, 1973; *Carr*, 1974; *Wilson and Head*, 1980; *Huppert and Sparks*, 1985; *Williams et al*., 1998, 2000, 2001, 2005; *Leverington*, 2004]. These lavas could have flowed either in subsurface lava tubes [e.g., *Greeley*, 1971a] or in leveed or eroded surface lava channels [*Hulme*, 1973, 1974, 1982; *Head and Wilson*, 1980; *Wilson and Head*, 1981; *Komatsu and Baker*, 1992; *Gregg and Greeley*, 1993; *Williams et al*., 1998, 2000, 2005; *Leverington*, 2004; *Hurwitz et al*., 2010, 2012, 2013]. Channels on the Moon with parallel, laterally continuous walls that extend into the substrate are interpreted to have formed as the result of erosion by lava flowing in a surface channel [*Hulme*, 1973; *Head and Wilson*, 1980; *Wilson and Head*, 1980; *Williams et al*., 2000; *Hurwitz et al*., 2012, 2013], and by analogy we consider the similar features observed on the surface of Mercury to represent candidates for channels that formed similarly by lava erosion (Figure 1).

[34] Another potential fluid that has been observed to carve channels is impact melt [e.g., *Howard and Wilshire*, 1973; *Bray et al.*, 2010]. Impact melt would be more likely to have a higher viscosity because of a higher particulate content [i.e., *Grieve and Cintala*, 1992, 1997; *Marion and Sylvester*, 2010] and to have been too limited in flux and volume to form the channels considered in this study. Moreover, although terrestrial particulate flows associated with base surges during phreatomagmatic eruptions [*Fisher*, 1977] and pyroclastic flows [*Sparks et al*., 1997] have been observed to erode furrows and U-shaped channels on Earth, these features tend to have depths of only 0.1–3 m rather than the hundreds of meters observed for channels on Mercury. Lava is considered a more probable erosional agent than impact melt in this study because lava is more likely to erupt at a higher temperature, with a lower viscosity, and at a sustained flux consistent with those predicted to be required to accommodate the characteristics of the observed channels.

[35] The features identified as candidate products of lava erosion can be separated into two size categories, including wide valleys having widths of at least ~18 km, and narrow channels with widths less than ~7 km (Table 1). Mathematical models for the formation of a representative wide valley and narrow channel indicate that lava with a composition similar to a low-viscosity komatiite would have eroded at a faster rate than lava with a composition similar to a low-iron equivalent of a terrestrial ocean island basalt. Results also indicate that thermal erosion dominated the lava erosion process during the formation of a narrow channel, but mechanical erosion was likely to have dominated the initial stages of formation of a wide valley when the substrate consisted of unconsolidated regolith material. The presence of this regolith layer would have reduced the time required to form the valley by lava erosion.

[36] The erosion rates predicted by these models to form the wide valley and the narrow channel by thermal erosion can be compared with results from similar analyses that have been conducted for channels on the Moon and Mars. It should be noted that modeled erosion rates are strongly dependent on channel morphology and the local geology relevant to each feature considered. The wide valley on Mercury modeled in detail here has a width (18 km) that is less than that of Athabasca Valles on Mars (27 km) and a depth (500 m) that is greater than that of Athabasca Valles (102 m). In addition, more lava is observed in the partially filled Kofi basin at the terminus of valley 1 on Mercury (1.5×10^4 km^3) than in the partially filled Cerberus Palus basin at the terminus of Athabasca Valles (5×10^3 km^3 [*Jaeger et al*., 2010]), a scenario that is consistent with the interpretation that more lava was required to form this particular valley on Mercury than the corresponding feature on Mars. With these differences, model results suggest that lava incised into the substrate by thermal erosion at a higher erosion rate (~3 m d^{-1} for a slope of ~0.3°) to form the valley observed near the northern volcanic plains on Mercury than that predicted for Athabasca Valles (0.9 m d^{-1}, [*Hurwitz and Head*, 2012]). Given two identical valleys on Mercury and on Mars, with identical widths, depths, regional slopes, and lava and substrate compositions, the modeled thermal erosion rates should be equivalent for the formation of both because the surface gravitational acceleration is nearly identical on the two planets.

[37] In contrast, the narrow channel on Mercury investigated here has a width (2800 m) that is similar to that of Rima Prinz (1800 m) on the Moon, a depth (420 m) that is greater than that of Rima Prinz (200 m), and a gradient (estimated at ~0.1°) that is likely to be less than for Rima Prinz (0.7°). No deposits associated with the terminus of either channel are observed, possibly the result of concealment by subsequent mare emplacement on the Moon or by younger impact craters on Mercury. With these differences, model results suggest that lava incised into the substrate by thermal erosion at only a slightly lower erosion rate (~1.0 m d^{-1}) to form the channel observed on Mercury than is predicted for Rima Prinz (1.7 m d^{-1} [*Hurwitz et al*., 2012]). If two identical channels were observed on Mercury and on the Moon, the modeled thermal erosion rates would be slightly lower in the lunar case because of the lower surface gravitational acceleration on the Moon. These results indicate that channel width strongly affects model results, particularly those predicting lava flow velocity. Specifically, the width of the comparison channel on the Moon was sufficiently narrower than the channel on Mercury to overcome the expected influence of gravity on the efficiency of thermal erosion rates.

[38] The fluxes required by the models to be consistent with the observed characteristics of the wide valley on Mercury, $(0.2–1.7) \times 10^6$ m^3 s^{-1} (Table 3), overlap both the range estimated for a terrestrial fissure eruption inferred to have produced the Teepee Butte Member of the Columbia River Basalts, $(0.1–1.2) \times 10^6$ m^3 s^{-1} [*Reidel and Tolan*,

1992], and the range calculated for a Martian fissure eruption inferred to have produced a lava flow through Athabasca Valles, $(5–20) \times 10^6\,m^3\,s^{-1}$ [*Jaeger et al*., 2010]. The eruption flux predicted for the formation of the valley on Mercury is therefore consistent with the emplacement of a local member of a flood lava unit. These high effusion rates are consistent with the proximity of the wide valleys to the northern volcanic plains, suggesting that the wide valleys may have formed in eruptions similar to and potentially contemporaneously with the eruptions that flooded the northern lowlands [*Head et al*., 2011; *Zuber et al*., 2012]. It should be noted that erosion by lava has not been documented in association with the Teepee Butte Member because terrestrial flood basalts are interpreted to have been emplaced by inflation processes rather than as the result of a turbulent flow [e.g., *Self et al.*, 1997]. Emplacement by inflation decreases the likelihood for erosion to occur during analogous terrestrial events. In contrast, the Martian flood basalt associated with Athabasca Valles has been interpreted to be the product of a rapid, turbulent effusion of lava [*Jaeger et al*., 2010], and so this Martian example may represent a more direct point of comparison with the wide valleys on Mercury.

[39] In contrast to the results for the large valley observed on Mercury, model results indicate that smaller fluxes are sufficient for the formation of the narrow channels on Mercury (i.e., $\sim 5100\,m^3\,s^{-1}$, Table 3). These smaller fluxes are consistent with those inferred for the formation of lunar sinuous rilles (e.g., $\sim 4400\,m^3\,s^{-1}$ for Rima Prinz) [*Head and Wilson*, 1980; *Wilson and Head*, 1980; *Hurwitz et al*., 2012]. The lunar sinuous rilles are thought to have formed as the result of a point-source eruption [e.g., *Wilson and Head*, 1981], supporting the inference that the narrow channels observed on Mercury may also have formed from more isolated, point-source eruptions of lava than the wider valleys.

6. Conclusions

[40] Observations of the surface of Mercury indicate that broad volcanic plains are the most widespread volcanic features and that associated constructional or erosional volcanic morphologies are rarely observed. However, several features have been identified that are consistent with erosion of the surface, potentially by lava. Results from numerical models of lava erosion indicate that thermal erosion dominated the formation of the wide valleys seen on Mercury, if they formed in a coherent substrate, but that mechanical erosion would have dominated initial channel formation if the lava encountered an upper layer of unconsolidated regolith. For one wide valley modeled in detail, the eruption may have originated in a pit at the northwestern end of the valley, and the required eruptive flux is comparable to that of the eruption of the terrestrial Teepee Butte Member that contributed to the formation of a flood basalt (the Columbia River Basalt). This type of eruption is consistent with the proximity of the wide valleys to the northern volcanic plains, interpreted to be the product of flood volcanism.

[41] In contrast, model results suggest that thermal erosion would have dominated the formation of narrow channels on Mercury regardless of substrate rigidity. The calculated eruption required to form the narrow channel on Mercury that we modeled in detail is consistent with a local point-source eruption (as has been inferred for lunar sinuous rilles). This eruption would form a feature that is more likely to be preserved in isolation of larger volcanic features such as large expanses of smooth plains that fill basins and bury smaller volcanic vents and channels. These results are consistent with observations of four narrow channels identified in the southern hemisphere of Mercury that are associated with the exterior of large impact structures much like Rima Prinz on the Moon. Although the results of this paper indicate how erosion by lava might have occurred on the surface of Mercury, other formation mechanisms for the observed channel features must also be considered. The wide valleys, for instance, may have formed from lava flooding terrain that was previously sculpted during the formation of the Caloris basin, and the narrow channels may have formed by the incision of impact melt into impact ejecta material. Further analysis is needed to distinguish among possible formational scenarios.

[42] **Acknowledgments**. We thank David Hollibaugh Baker and Jay Dickson for their tireless efforts in downloading and processing MESSENGER data, and we thank Karen R. Stockstill-Cahill for insightful suggestions during the preparation of this work. We also thank David A. Williams and Tracy K. P. Gregg for constructive reviews. Finally, we acknowledge the MESSENGER team for their ingenuity in getting us to Mercury in the first place. The MESSENGER project is supported by the NASA Discovery Program under contracts NAS5-97271 to The Johns Hopkins University Applied Physics Laboratory and NASW-00002 to the Carnegie Institution of Washington.

References

Baker, D. M. H., J. W. Head, S. C. Schon, C. M. Ernst, L. M. Prockter, S. L. Murchie, B. W. Denevi, S. C. Solomon, and R. G. Strom (2011), The transition from complex crater to peak-ring basin on Mercury: New observations from MESSENGER flyby data and constraints on basin formation models, *Planet. Space Sci.*, *59*, 1932–1948.

Bray, V. J., et al. (2010), New insight into lunar impact melt mobility from the LRO camera, *Geophys. Res. Lett.*, *37*, doi:10.1029/2010GL044666.

Byrne, P. K., C. Klimczak, B. W. Denevi, T. R. Watters, S. C. Solomon, A. C. Enns, J. W. Head, D. M. Hurwitz, and D. M. H. Baker (2011), Surface lava flow features on Mercury, *Abstracts with Programs, 43*, paper 142–7, p. 358, Geological Society of America, Boulder, Colo.

Byrne, P. K., C. Klimczak, D. A. Williams, D. M. Hurwitz, S. C. Solomon, J. W. Head, F. Preusker, and J. Oberst (2013), An assemblage of lava flow features on Mercury, *J. Geophys. Res.*, doi:10.1029/2012JE004197.

Carr, M. H. (1974), The role of lava erosion in the formation of lunar rilles and Martian channels, *Icarus*, *22*, 1–23.

Carr, M. H., and G. D. Clow (1981), Martian channels and valleys: Their characteristics, distribution, and age, *Icarus*, *48*, 91–117.

Clague, D. A., W. S. Weber, and J. E. Dixon (1991), Picritic glasses from Hawaii, *Nature*, *353*, 553–556.

Dzurisin, D. (1978), The tectonic and volcanic history of Mercury as inferred from studies of scarps, ridges, troughs, and other lineaments, *J. Geophys. Res.*, *83*, 4883–4906.

Fa, W., and Y. Q. Jin (2010), A primary analysis of microwave brightness temperature of lunar surface from Chang-E 1 multi-channel radiometer observation and inversion of regolith layer thickness, *Icarus*, *207*, 605–615.

Fagents, S. A., and R. Greeley (2001), Factors influencing lava-substrate heat transfer and implications for thermomechanical erosion, *Bull. Volcanol.*, *62*, 519–532.

Fassett C. I., J. W. Head, D. T. Blewett, C. R. Chapman, J. L. Dickson, S. L. Murchie, S. C. Solomon, and T. R. Watters (2009), Caloris impact basin: Exterior geomorphology, stratigraphy, morphometry, radial sculpture, and smooth plains deposits, *Earth Planet. Sci. Lett.*, *285*, 297–308.

Fassett, C. I., B. W. Denevi, J. L. Whitten, T. A. Goudge, D. M. H. Baker, D. M. Hurwitz, L. R. Ostrach, Z. Xiao, P. K. Byrne, and C. Klimczak (2011), Widespread and voluminous flood volcanism in the northern lowlands of Mercury revealed by MESSENGER, *Abstracts with Programs, 43*, paper 142-6, p. 358, Geological Society of America, Boulder, Colo.

Fisher, F. V. (1977), Erosion by volcanic base-surge density currents: U-shaped channels, *Geol. Soc. Amer. Bull.*, *88*, 1287–1297.
Goncharov, V. N. (1964), *Dynamics of Channel Flow*, pp. 317, translated from Russian by Israel Program Sci. Transl., U. S. Dep. Of Commer., Off. Of Tech. Serv., Washington, D. C.
Greeley, R. (1971a), Lunar Hadley rille: Considerations of its origin, *Science*, *172*, 722–725.
Greeley, R. (1971b), Lava tubes and channels in the lunar Marius Hills, *Earth Moon Planets*, *3*, 289–314.
Gregg, T. K. P., and R. Greeley (1993), Formation of venusian canali: Considerations of lava types and their thermal behaviors, *J. Geophys. Res.*, *98*, 10,873–10,882.
Grieve, R. A. F., and M. J. Cintala (1992), An analysis of differential impact melt-crater scaling and implications for the terrestrial impact record, *Meteoritics*, *27*, 526–538.
Grieve, R. A. F., and M. J. Cintala (1997), Planetary difference in impact melting, *Adv. Space Res.*, *20*, 1551–1560.
Hartmann, W. K. (1973), Ancient lunar mega-regolith and subsurface structure, *Icarus*, *18*, 634–636.
Head, J. W. (1976), Lunar volcanism in space and time, *Rev. Geophys. Space Phys.*, *14*, 265–300.
Head, J. W., and L. Wilson (1980), The formation of eroded depressions around the sources of lunar sinuous rilles: Observations, *Lunar Planet. Sci.*, *11*, 426–428.
Head, J. W., and L. Wilson (1986), Volcanic processes and landforms on Venus: Theory, predictions, and observations, *J. Geophys. Res.*, *91*, 9407–9446.
Head, J. W., and L. Wilson (1992), Lunar mare volcanism: Stratigraphy, eruption conditions, and the evolution of secondary crusts, *Geochim. Cosmochim. Acta*, *56*, 2155–2175.
Head, J. W., L. S. Crumpler, J. C. Aubele, J. E. Guest, and R. S. Saunders (1992), Venus volcanism: Classification of volcanic features and structures, associations, and global distribution from Magellan data, *J. Geophys. Res.*, *97*, 13,153–13,197.
Head, J. W., et al. (2009),Volcanism on Mercury: Evidence from the first MESSENGER flyby for extrusive and explosive activity and the volcanic origin of plains, *Earth Planet. Sci. Lett.*, *285*, 227–242.
Head, J. W., et al. (2011), Flood volcanism in the northern high latitudes of Mercury revealed by MESSENGER, *Science*, *333*, 1853–1856.
Hiesinger, H., and J. W. Head (2006), New views of lunar geoscience: An introduction and overview, *Rev. Mineral. Geochem.*, *60*, 1–85.
Hörz, F., R. Grieve, G. Heiken, P. Spudis, and A. Binder (1991), Lunar surface processes, in *Lunar Sourcebook: A User's Guide to the Moon*, edited by G. H. Heiken, D. T. Vaniman, and B. M. French, pp. 61–120, Cambridge University Press, New York.
Howard, K. A., and H. G. Wilshire (1973), Flows of impact melt at lunar craters, *Lunar Sci.*, *4*, 389–390.
Hulme, G. (1973), Turbulent lava flow and the formation of lunar sinuous rilles, *Mod. Geol.*, *4*, 107–117.
Hulme, G. (1974), The interpretation of lava flow morphology, *Geophys. J. Int.*, *39*, 361–383.
Hulme, G. (1982), A review of lava flow processes related to the formation of lunar sinuous rilles, *Geophys. Surv.*, *5*, 245–279.
Huppert, H. E., and S. J. Sparks (1985), Komatiites I: Eruption and flow, *J. Petrol.*, *26*, 694–725.
Hurwitz, D. M., and J. W. Head (2012), Testing the late-stage outflow channel origin hypothesis: Investigating both water erosion and lava erosion origin for Athabasca Valles, Mars, *Lunar Planet. Sci. Conf.*, *43*, abstract 1056.
Hurwitz, D. M., C. I. Fassett, J. W. Head, and L. Wilson (2010), Formation of an eroded lava channel within an Elysium Planitia impact crater: Distinguishing between a mechanical and thermal origin, *Icarus*, *210*, 626–634.
Hurwitz, D. M., J. W. Head, L. Wilson, and H. Hiesinger (2012), Origin of lunar sinuous rilles: Modeling effects of gravity, surface slope, and lava composition on erosion rates during the formation of Rima Prinz, *J. Geophys. Res.*, *117*, E00H14, doi:10.1029/2011JE004000.
Hurwitz, D. M., J. W. Head, and H. Hiesinger (2013), Lunar sinuous rilles: Distribution, characteristics, and implications for their origin, *Planet. Space Sci.*, doi:http://dx.doi.org/10.1016/j.pss.2012.10.019, in press.
Jaeger, W. L., et al. (2010), Emplacement of the youngest flood lava on Mars: A short, turbulent story, *Icarus*, *205*, 230–243.
Kakaç, S., R. K. Shah, and W. Aung (1987), *Handbook of Single-Phase Convective Heat Transfer*, John Wiley, New York, 1238 pp.
Keszthelyi, L., and S. Self (1998), Some physical requirements for the emplacement of long basaltic lava flows, *J. Geophys. Res.*, *103*, 27,447–27, 464.
Kiefer, W. S., and B. C. Murray (1987), The formation of Mercury's smooth plains, *Icarus*, *72*, 477–491.
Kobayashi, T., J. H. Kim, S. R. Lee, H. Araki, and T. Ono (2010), Simultaneous observation of Lunar Radar Sounder and Laser Altimeter of Kaguya for lunar regolith layer thickness estimate, *Geosci. Remote Sens. Lett. IEEE*, *7*, 435–439.
Komatsu, G., and V. R. Baker (1992), Venusian sinuous rilles, in *Papers Presented to the International Colloquium on Venus*, pp. 60–61, Lunar and Planetary Institute, Houston, Tex.
Komatsu, G., J. S. Kargel, and V. R. Baker (1992), Canali-type channels on Venus: Some genetic constraints, *Geophys. Res. Lett.*, *19*, 1415–1418.
Komatsu, G., V. R. Baker, V. C. Gulick, and T. J. Parker (1993), Venusian channels and valleys: Distribution and volcanological implications, *Icarus*, *102*, 1–25.
Lesher, C. M., and N. T. Arndt (1995), REE and Nd isotope geochemistry, petrogenesis and volcanic evolution of contaminated komatiites at Kambalda, Western Australia, *Lithos*, *34*, 127–157.
Leverington, D. W. (2004), Volcanic rilles, streamlined islands, and the origin of outflow channels on Mars, *J. Geophys. Res.*, *109*, E10011, doi:10.1029/2004JE002311.
Marion, C. L., and P. J. Sylvester (2010), Composition and heterogeneity of anorthositic impact melt at Mistastin Lake crater, Labrador, *Planet. Space Sci.*, *58*, 552–573.
Masursky, H., J. M. Boyce, A. L. Dial, G. G. Schaber, and M. E. Strobell (1977), Classification and time of formation of martian channels based on Viking data, *J. Geophys. Res.*, *82*, 4016–4038.
Morrison, D. (1970), Thermophysics of the planet Mercury, *Space Sci. Rev.*, *11*, 271–307.
Murray, B. C., R. G. Strom, N. J. Trask, and D. E. Gault (1975), Surface history of Mercury: Implications for terrestrial planets, *J. Geophys. Res.*, *80*, 2508–2514.
Nittler, L. R., et al. (2011), The major-element composition of Mercury's surface from MESSENGER X-Ray Spectrometer, *Science*, *333*, 1847–1850.
Oberbeck, V. R., W. L. Quaide, R. E. Arvidson, and H. R. Aggarwal (1977), Comparative studies of lunar, martian, and mercurian craters and plains, *J. Geophys. Res.*, *82*, 1681–1698.
Paige, D. A., M. A. Siegler, J. K. Harmon, D. E. Smith, M. T. Zuber, G. A. Neumann, and S. C. Solomon (2012), Thermal stability of frozen volatiles in the north polar region of Mercury, *Lunar Planet. Sci.*, *43*, 2875.
Prockter, L. M., et al. (2010), Evidence for young volcanism on Mercury from the third MESSENGER flyby, *Science*, *329*, 668–671.
Reidel, S. P., and T. L. Tolan (1992), Eruption and emplacement of flood basalt: An example from the large-volume Teepee Butte Member, Columbia River Basalt Group, *Geol. Soc. Amer. Bull.*, *104*, 1650–1671.
Robinson, M. S., and P. G. Lucey (1997), Recalibrated Mariner 10 color mosaics: Implications for mercurian volcanism, *Science*, *275*, 197–200.
Schon, S. C., J. W. Head, D. M. H. Baker, C. M. Ernst, L. M. Prockter, S. L. Murchie, and S. C. Solomon (2011), Eminescu impact structure: Insight into the transition from complex crater to peak-ring basin on Mercury, *Planet. Space Sci.*, *59*, 1949–1959.
Self, S., T. Thordarson, and L. Keszthelyi (1997), Emplacement of continental flood basalt lava flows, *Geophys. Mono., Amer. Geophys. Union*, *100*, 381–410.
Sharp, R. P., and M. C. Malin (1975), Channels on Mars, *Geol. Soc. Amer. Bull.*, *86*, 593–609.
Sklar, L., and W. E. Dietrich (1998), River longitudinal profiles and bedrock incision models: Stream power and the influence of sediment supply, in *Rivers Over Rock*, edited by K. J. Tinkler and E. E. Wohl, pp. 237–260, AGU, Washington, D.C.
Solomon, S. C., et al. (2012), Long-wavelength topographic change on Mercury: Evidence and mechanisms, *Lunar Planet. Sci.*, *43*, 1578.
Sparks, R. S. J., M. C. Gardeweg, E. S. Calder, and S. J. Matthews (1997), Erosion by pyroclastic flows on Lascar Volcano, Chile, *Bull. Volcanol.*, *58*, 557–565.
Strain, P. L., and F. El-Baz (1977), Topography of sinuous rilles in the Harbinger Mountains region of the Moon, *Earth Moon Planets*, *16*, 221–229.
Strom, R. G. (1977), Origin and relative age of lunar and mercurian intercrater plains, *Phys. Earth Planet. Inter.*, *15*, 156–172.
Strom, R. G., N. J. Trask, and J. E. Guest (1975), Tectonism and volcanism on Mercury, *J. Geophys. Res.*, *80*, 2478–2507.
Trask, N. J., and J. E. Guest (1975), Preliminary geologic terrain map of Mercury, *J. Geophys. Res.*, *80*, 2461–2477.
Watters, T. R., S. C. Solomon, M. S. Robinson, J. W. Head, S. L. André, S. A. Hauck II, and S. L. Murchie (2009a), The tectonics of Mercury: The view after MESSENGER's first flyby, *Earth Planet. Sci. Lett.*, *285*, 283–296.
Watters, T. R., S. L. Murchie, M. S. Robinson, S. C. Solomon, B. W. Denevi, S. L. André, and J. W. Head (2009b), Emplacement and tectonic deformation of smooth plains in the Caloris basin, Mercury, *Earth Planet. Sci. Lett.*, *285*, 309–319.
Weider, S. Z., L. R. Nittler, R. D. Starr, T. J. McCoy, K. R. Stockstill-Cahill, P. K. Byrne, B. W. Denevi, J. W. Head, and S. C. Solomon (2012),

Chemical heterogeneity on Mercury's surface revealed by the MESSENGER X-Ray Spectrometer, *J. Geophys. Res.*, doi:10.1029/2012JE004153.

Whitford-Stark, J. L., and J. W. Head (1977), The Procellarum volcanic complexes: Contrasting styles of volcanism, *Lunar Sci.*, *8*, 2705–2724.

Whitten, J. L., J. W. Head, M. I. Staid, C. M. Pieters, J. F. Mustard, R. Clark, J. W. Nettles, R. L. Klima, and L. A. Taylor (2011), Lunar mare deposits associated with the Orientale impact basin: New insights into mineralogy, history, mode of emplacement, and relation to Orientale Basin evolution from Moon Mineralogy Mapper (M^3) data from Chandrayaan-1, *J. Geophys. Res.*, *116*, E00G09, doi:10.1029/2010JE003736.

Wilhelms, D. E. (1976), Mercurian volcanism questioned, *Icarus*, *28*, 551–558.

Williams, D. A., R. C. Kerr, and C. M. Lesher (1998), Emplacement and erosion by Archean komatiite lava flows at Kambalda: Revisited, *J. Geophys. Res.*, *103*, 27,533–27,549.

Williams, D. A., S. A. Fagents, and R. Greeley (2000), A reassessment of the emplacement and erosional potential of turbulent, low-viscosity lavas on the Moon, *J. Geophys. Res.*, *105*, 20,189–20,205.

Williams, D. A., R. C. Kerr, C. M. Lesher, and S. J. Barnes (2001), Analytical/numerical modeling of komatiite lava emplacement and thermal erosion at Perseverance, Western Australia, *J. Volcanol. Geotherm. Res.*, *110*, 27–55.

Williams, D. A., R. Greeley, E. Hauber, K. Gwinner, and G. Neukum (2005), Erosion by flowing martian lava: New insights for Hecates Tholus from Mars Express and MER data, *J. Geophys. Res.*, *110*, E05006, doi:10.1029/2004JE002377.

Wilson, L., and J. W. Head (1980), The formation of eroded depressions around the sources of lunar sinuous rilles: Theory, *Lunar Planet. Sci.*, *11*, 1260–1262.

Wilson, L., and J. W. Head (1981), Ascent and eruption of basaltic magma on the Earth and Moon, *J. Geophys. Res.*, *86*, 2971–3001.

Wilson, L., and J. W. Head (1997), Factors controlling the depths and sizes of magma reservoirs in martian volcanoes, *Lunar Planet. Sci.*, *28*, 1284.

Wilson, L., and J. W. Head (2012), Volcanic eruption processes on Mercury, *Lunar Planet. Sci.*, *43*, 1316.

Zuber, M. T., et al. (2010), Accommodation of lithospheric shortening on Mercury from altimetric profiles of ridges and lobate scarps measured during MESSENGER flybys 1 and 2, *Icarus*, *209*, 247–256.

Zuber, M. T., et al. (2012), Topography of the northern hemisphere of Mercury from MESSENGER Laser Altimetry, *Science*, *336*, 217–220, doi:10.1126/science.1218805.